TWO-LAYER SHALLOW WATER MODELLING OF FAST GEOMORPHIC FLOWS AND EXPERIMENTAL VALIDATION ON IDEALISED LABORATORY DAM-BREAK WAVES

BENOIT SPINEWINE

FSR Research Fellow, Department of Civil & Environmental Engineering,
Universite catholique de Louvain, Place du Levant 1, BE 1348 Louvain-la-Neuve, Belgium
(Tel: +32-10-47-21-23, Fax: +32-10-47-21-79, e-mail: spinewine@gce.ucl.ac.be)

Abstract

Fast geomorphic floods, as resulting from dam- or dike breaks and debris flows, may induce severe soil movements that in turn affect the wave dynamics in terms of arrival times and attained levels. They involve the movement of dense solid-fluid mixtures that may reasonably be assumed to behave as an equivalent continuum. A multi-phase approach is adopted to develop a set of governing equations that rely on a two-layer shallow water description. The proposed framework accounts for granular phase dilatation resulting from grain entrainment across the bed interface, and for the related mass and momentum exchanges induced between the flowing layers. Erosion and deposition derives from a theoretical shock relation, so that the closures for shear stresses at the interfaces govern both frictional losses and geomorphic exchanges in a unified description. The governing equations are solved in a finite volume numerical scheme, both in a 1D version on Cartesian grids and in a 2D version on unstructured triangular meshes. Numerical simulations are faced with results of idealised laboratory experiments of dam-break waves in two configurations: the 1D version is tested against experiments involving a bed profile with an initial discontinuity at the dam location; the 2D version is faced to a sudden valley enlargement in the downstream reach.

Keywords: Dam-break; Movable bed; Two-layer shallow-water model; Laboratory experiments

1. INTRODUCTION

Catastrophic floods are often associated with the mobilisation of large amounts of sediments, in a variety of forms ranging from mountainous debris flows to dam- or dike-breaches and mud-flows, ... A recent example is the 1996 Lake Ha!Ha! dam-break flood, involving intense geomorphic action along the whole 30 kilometres of the Ha!Ha! River downstream of the failed dam, with channel widening up to locally 700 %, a large-scale avulsion, local erosion of a 20 metres-deep layer of glacial deposits, and intense deposition areas at the entrance of the Ha!Ha! Bay (Brooks and Lawrence, 1999). Even when involving smaller volumes of material, geomorphic interactions can lead to severe consequences because of localised changes or adverse secondary effects. In the 1980 Pollalie Creek event, Oregon, for instance, the material entrained by a debris flow deposited in a downstream reach, forming a dam that ultimately failed and caused severe flooding (Gallino and Pierson, 1985).

Accounting for sediment movement and associated geomorphic changes in flood simulations seems crucial for at least two reasons. Firstly the altered valley configuration provides changing boundary conditions to which the flow is continuously adjusting. Landscape reshaping may significantly increase resulting flood damages, like in case of massive bank erosion, failure of infrastructures or severe deposits of fine sediments in flatter areas. No less importantly however, through friction, inertial effects and momentum exchanges with the fluid phase, erosion of bed material may in turn significantly affect the dynamics of flood wave development in terms of arrival time of the wave front and envelope of maximum attained flood levels, two parameters of utmost importance for emergency planning, risk management and damage assessment.

We propose a simple though robust theoretical framework for the simulation of fast geomorphic flows involving intense geomorphic action and sediment transport moving as a dense contact load, and we present two series of 1D and 2D idealised laboratory dam-break experiments on movable beds in different configurations, whose observations are faced with numerical simulations based on the above approach. The latter relies on a multi-layer shallow water description and follows hereby the work by Capart and Young (2002) or Fraccarollo et al. (2003). In contrast with previous works however, we account explicitly for the change in solid concentration resulting from entrainment/deposition of solid material, as well as the related mass and momentum exchanges between the transport and water layers. A simple slope failure mechanism is implemented to account for local bed or bank failures due to geotechnical instabilities. In section 2 of the paper we establish the set of governing equations. The computational methodology is briefly presented. In section 3 the two series of laboratory dam-break experiments are presented. The first configuration involves a prismatic dam-break wave over a bed profile with an initial bed level discontinuity at the dam location. The second explores the case of a sudden asymmetrical valley enlargement in the downstream reach. Experimental observations are compared with numerical simulations in section 4.

2. MATHEMATICAL FRAMEWORK

2.1 PHENOMENOLOGICAL AND MATHEMATICAL DESCRIPTION

We rely on a vertical flow structure similar to that postulated by Capart and Young (2002), as sketched in Figure 1. The flow is subdivided in three different layers, each having homogeneous properties: the static granular bed at level z_b, a transport layer of depth h_s made of a moving water/sediments slurry, and a pure water layer of depth h_w on top.

The two moving layers are allowed to flow at distinct velocities u_w and u_s. The proposed description makes no a priori assumption on the ratio between layer velocities. This ratio is rather governed by the physical processes of frictional exchanges and inter-layer mass and momentum transfers. In the two-dimensional extension of the description, the two layers are further allowed to flow in different directions according to their velocity components (u_w,v_w) and (u_s,v_s). This turns to be a key advantage compared to other formulations (Cao and Carling, 2004; Ferreira et al., 2003) in which flow directions are locked together as a result of model

assumptions. Indeed, deviations between transport and water layer directions in case of strong geometrical discontinuities (as the sudden enlargement presented in section 3.2) or over complex topographies, may result in very different erosion and deposition patterns.

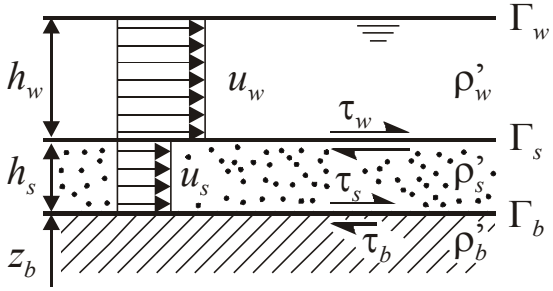

Fig. 1 Idealised layered flow structure

Erosion or deposition is viewed as a vertical movement of the interface $_b$, associated with a phase change of the granular material that undergoes a transition from a solid-like to a fluid-like behaviour (Capart, 2000).

In contrast with Capart and Young (2002), the bed and transport layer are now also characterised by distinct granular concentrations C_b and C_s. The main motivation for this postulate comes from the fact that erosion, associated with entrainment of material through the bed interface, requires a dilatation of the granular matrix, hence a reduction of its granular packing, even for highly concentrated flows. Recent stereoscopic measurements of dense debris flows (Spinewine et al. 2003) revealed that the net reduction of concentration resulting from inter-particle contacts in a dense collisional granular layer is substantial, and certainly higher than what one would derive from a quick visual observation of the flow.

This vertical expansion of the granular bed requires a net supply of water relative to the grains, to counterbalance the increase of void fraction. The opposite occurs in case of deposition, when the excess of water due to the reduction of pore volumes should be evacuated. In both cases, the shortage/excess in water content within the transport layer must be counter-balanced by water exchanges with the overlying pure water layer. As a result, geomorphic action is thus associated not only with mass and momentum exchanges across the bed interface, but also across the interface separating the two flow layers. This is opposed to previous formulations in which the two flow regions were supposed immiscible, and momentum transfer resulted only from frictional resistance at the interface. Erosion now induces an increase of the total transport-layer momentum resulting from an appeal of water from the faster water-layer overlying it. These mass and momentum exchanges are explicitly accounted for in the equations. Their implications on the flow dynamics vanish for equilibrium situations. On the contrary, they are substantial in case of highly transient flows with non-equilibrium sediment transport, as is the case for dam-break waves or debris flows.

Application of mass and momentum balances to the three different layers yield the following set of governing equations:

$$\frac{\partial h_w}{\partial t} + \frac{\partial}{\partial x}(h_w u_w) = -e_b \frac{C_b - C_s}{C_s} \quad , \quad \frac{\partial h_s}{\partial t} + \frac{\partial}{\partial x}(h_s u_s) = e_b \frac{C_b}{C_s} \quad , \quad \frac{\partial z_b}{\partial t} = -e_b \qquad (1a\text{-}c)$$

$$\frac{\partial(h_w u_w)}{\partial t}+\frac{\partial}{\partial x}\left(h_w u_w^2+\frac{g h_w^2}{2}\right)+g h_w\frac{\partial}{\partial x}(z_b+h_s)=-\frac{\tau_w}{\rho'_w}-e_b\frac{C_b-C_s}{C_s}\begin{pmatrix}u_w \text{ if } e_b>0\\ u_s \text{ if } e_b<0\end{pmatrix} \quad (2a)$$

$$\frac{\partial(h_s u_s)}{\partial t}+\frac{\partial}{\partial x}\left(h_s u_s^2+\frac{g h_s^2}{2}\right)+g h_s\left(\frac{\partial z_b}{\partial x}+\frac{\rho'_w}{\rho'_s}\frac{\partial h_w}{\partial x}\right)=\frac{\tau_w}{\rho'_s}-\frac{\tau_b}{\rho'_s}+\frac{\rho'_w}{\rho'_s}\frac{C_b-C_s}{C_s}e_b\begin{pmatrix}u_w \text{ if } e_b>0\\ u_s \text{ if } e_b<0\end{pmatrix} \quad (2b)$$

where $\rho'_w=\rho_w$ is the mass density of water, $\rho'_s=\rho_w(1-C_s)+\rho_s C_s$ is the mass density of the water-sediment mixture in the transport layer (ρ_s being the mass density of sediment particles), e_b is the erosion rate, and an asymmetry between erosion and deposition appears in the momentum equations to account for the correct momentum flux due to the exchange of water between the two moving layers.

Shear stresses are as shown in Figure 1. Note the discontinuous shear stress across the bottom interface $_b$, $_s$ being the entraining shear stress in the fluid-like region, and $_b$ the resisting shear stress in the solid-like granular bed. Expressing the jump condition for local conservation of longitudinal momentum across the bed interface yields, after manipulation, a theoretically-grounded criterion for the erosion rate

$$e_b=\frac{1}{\rho'_b|u_s|}(\tau_s-\tau_b) \quad (3)$$

where $\rho'_b=\rho_w(1-C_b)+\rho_s C_b$ is the mass density of the bed, including interstitial water. Erosion or deposition is thus initiated by an imbalance between shear stresses experienced on both sides of the bed interface.

The right-hand-side term of (1a) expresses the loss of mass in the water layer supplied to the transport layer in case of erosion. It vanishes if assuming equal sediment concentrations C_b=C_s. The right-hand-side term of (1b), on the other hand, accounts both for mass exchanges with the underlying bed and with the above water layer. It resumes to e_b in case of equal concentrations. Besides frictional interactions, special care has to be taken while expressing the morphodynamic momentum exchanges between the moving layers. The resulting asymmetry in case of erosion/deposition is important to be sure that the water transferred from the top layer to the transport layer or vice versa, travels with its proper velocity u_w or u_s.

All together, equations (1), (2) and (3) provide 6 equations for the 9 unknowns [z_b h_s h_w u_s u_w e_b $_b$ $_s$ $_w$]. We use closure relations for the shear stresses similar to those proposed by Capart and Young (2002):

$$\tau_w=\rho'_w C_{fw}(u_w-u_s)^2 \quad , \quad \tau_s=\rho'_s C_{fs} u_s^2 \quad , \quad \tau_b=c+\sigma'\tan\phi \quad (4)$$

The first two are fluid-like shear relations function of the square of the velocity jump at the interface. The last is a solid-like Coulomb criterion expressing the resisting shear stress as a function of Terzaghi's effective normal stress $\sigma'=(\rho'_s-\rho_w)g h_s$ and soil friction angle .

An additional operator is implemented to account for geostatic slope instabilities and failures, as described in more detail in Spinewine et al. (2002). Basically, the operator initiates slope failures wherever and whenever the local slope of the bed profile exceeds a predefined critical angle, and fluidises the bed material above a predefined residual angle starting at the toe of the failure surface. Both angles may not be equal, creating a metastable situation in between. Fluidisation is materialised simply by a transfer from the bed region to the transport

layer. In the present case of differing solid concentrations in those two layers, special care again has to be taken to insure consistency of mass and momentum balances in the two flow regions. The operator was initially designed for modelling lateral bank failures (Spinewine et al., 2002); in the context of the 'stepped' dam-break experiment presented in section 3a, it successfully reproduced the initial failure and reshaping of the bed discontinuity at the dam.

2.2 NUMERICAL SCHEME

The set of equations (1)-(2) may be written in the vector form

$$\frac{\partial \mathbf{U}}{\partial t} + \frac{\partial \mathbf{F}}{\partial x} + \mathbf{G}\frac{\partial \mathbf{U}}{\partial x} = \mathbf{H} \tag{5}$$

where the first term is the evolution of the conservation variables $\mathbf{U} = (z_b \; h_s \; h_w \; h_s u_s \; h_w u_w)^{\mathrm{T}}$, the second is the space derivative of flux vector $\mathbf{F}(\mathbf{U})$, the third accounts for non-conservative products through Jacobian matrix $\mathbf{G}(\mathbf{U})$, and $\mathbf{H}(\mathbf{U})$ represent the source terms.

We adopt a first-order accurate finite volume discretisation of (5). The 1D code uses a regular mesh with constant cell size *dx*, and for the integration of $\mathbf{F}(\mathbf{U})$ and $\mathbf{G}(\mathbf{U})$, it is largely derived from a model developed by H. Capart at National Taiwan University (Capart and Young, 2002), that was kindly made available to us. The 2D extension relies on an unstructured triangular mesh and solves the 1D Riemann problems in the direction orthogonal to every cell face. The architecture of the code is built on the skeleton of a one-layer model on a fixed bed, developed by V. Guinot at Université Montpellier II (Guinot, 2003), again kindly made available to us. For both versions, the hyperbolic operator – left-hand side of (6) – is integrated using the Godunov scheme of Harten, Lax & Van Leer with a lateralisation of the topographical non-conservative products (Fraccarollo et al., 2003). Integration of the various source terms is performed separately with an implicit Backward Euler scheme for stability.

3. IDEALISED LABORATORY DAM-BREAK EXPERIMENTS

We now present two series of small-scale laboratory dam-break waves performed on movable beds with different configurations, for which comparisons with model simulations are presented in section 4. The first configuration is one-dimensional, with a bed profile presenting a discontinuity across the dam. The higher bed levels in the upstream reach provide a rough analogue to reservoirs partially filled with sediments that are remobilised during the dam-break. The second configuration has a completely flat bed profile, but with a sudden channel enlargement to twice its width at some distance along the downstream reach. The objective was to investigate erosion and deposition patterns induced when a dam-break wave confined in a narrow valley invades a wider area.

The tests were performed in a new flume designed at the Civil Engineering Department (Fig. 2a). The flume is 6 m long, 0.25 m wide and 0.7 m high, and was specifically designed for idealised dam-break experiments on movable beds. Breaking of the dam is simulated by the rapid downward movement of a thin gate at the middle of the flume, entrained by a pneumatic jack. Opening time in the order of 0.1 s is achieved over the full nominal height of

50 cm. As opposed to a rising gate used in previous experiments, the direction of gate movement was chosen here to provide better-defined initial conditions (Fig. 2b and c).

Initial test conditions for the two configurations are summarised in Figure 3.

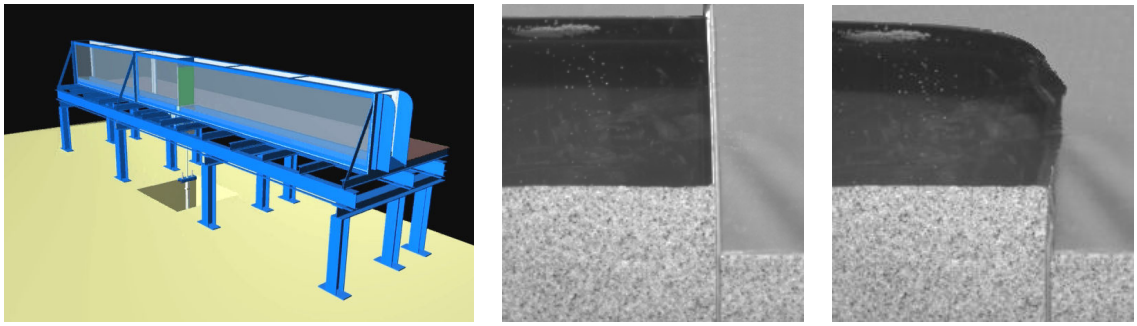

Fig. 2a-c Flume for idealised dam-break experiments, here in the prismatic configuration. a: upstream 3D view. b and c: close-ups of the flow during gate opening: initial condition (b) and nearly unperturbed water body after gate removal (c).

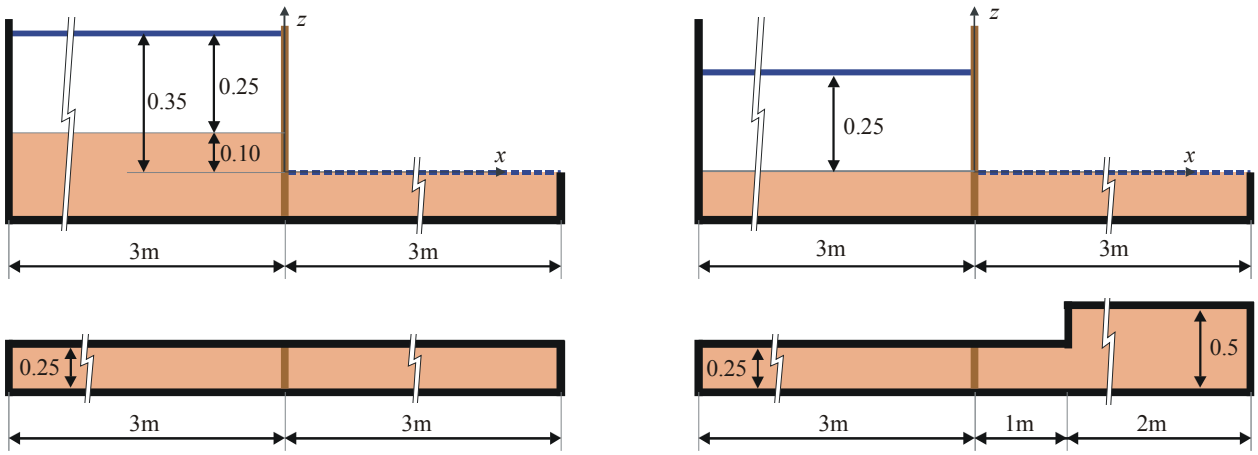

Fig. 3 Initial conditions for the dam-break wave experiments. Left: prismatic configuration with a bed level discontinuity; right: flat bed configuration with a sudden channel enlargement. Top: elevations; bottom: plan views. All dimensions in metres.

3.1 1D DAM-BREAK WITH AN INITIAL BED DISCONTINUITY

Tests were performed with uniform sand having grain sizes in the range 1 to 2 millimetres. More details about this configuration as well as similar tests performed with a lighter sediment analogue may be found in the companion paper by Spinewine and Zech (2005). The initial conditions were as sketched in the left panes of Figure 3. The initial bed profile features horizontal reaches upstream and downstream, with an initial discontinuity at the gate section, so that the upstream level is initially $h_{s,0} = 10$ cm higher than the downstream level. In the upstream reservoir, an additional layer of 25 cm of pure water at rest is provided, so that the total head upstream is $h_0 = 35$ cm. Instrumentation of the tests consist in fast digital imaging through the transparent sidewalls and bulk sediment measurements at the flume outlet. To guarantee a sufficient degree of detail with the limited resolution of the camera, identical tests were repeated in successive steps by translating the camera by multiples of 75 cm. The

images corresponding to the various camera positions but pertaining to the same instant were then rearranged and merged to form full flow mosaics over the entire flume length.

The relevant flow interfaces (water profile; upper limit of transport layer; boundary between moving and static grains) are positioned by a semi-manual procedure, described in Spinewine and Zech, 2005. Bulk measurements delivered the total mass of bed material transported by the dam-break wave and collected at the flume outlet.

Fig. 4 shows full flow mosaics at selected instants. During the initial stages of wave formation, massive soil movements occur around the bed step. The vertical step exceeds the repose angle of the bed material, resulting in an instability and mass failure. A substantial volume of soil around the initial step is liquefied (see Fig. 4a). The plastic behaviour of this soil movement has little to do with traditional sediment transport mechanisms, but may be accounted for with the geostatic operator described in section 2. In a second phase, a stable wavefront develops, saturated with sediments. Bed material continues to be incorporated in the flow as the front progresses. In a third phase, the wavefront tends to decelerate and the intensity of transport decreases. Partial re-deposition of sediments occurs in the first reaches.

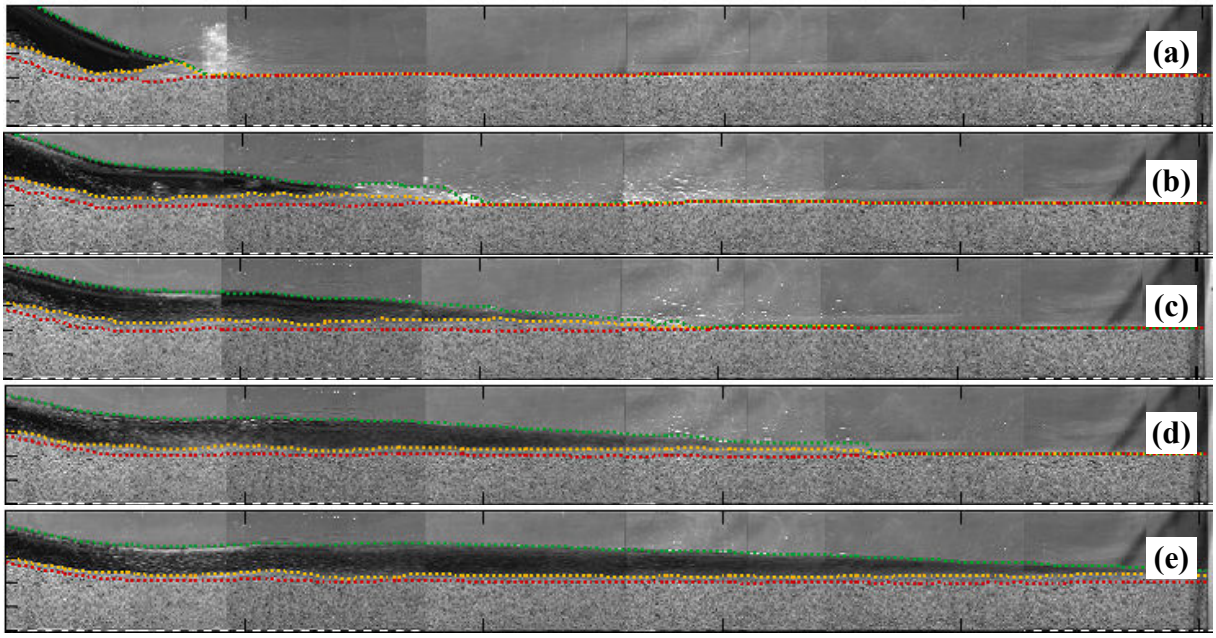

Fig. 4 Reconstructed flow mosaics for the 1D tests at t = 0.25, 0.5, 0.75, 1.0 and 1.5 s. Green, yellow and red lines indicate the profiles of water, transport layer and sediment bed levels. On the upstream side, the flow is more gentle. We observed the gradual formation of a weak hydraulic jump.

3.2 2D DAM-BREAK WITH A SUDDEN CHANNEL ENLARGEMENT

The 2D configuration consist in a sudden enlargement at a station one metre downstream of the dam. The width grows from 0.25m to 0.5m, and the widening is confined on one side of the channel, making the configuration asymmetrical (see the right panes of Fig.3).

Digital images of the flow were acquired both through the sidewalls and from the top. Fig.5 show top views at selected instants t = 0.5, 1.0 and 2.0 seconds (Fig. 5a-c respectively),

as well as an impression of the final topography captured while the bed gradually emerges as the residual water is drained out (Fig. 5d).

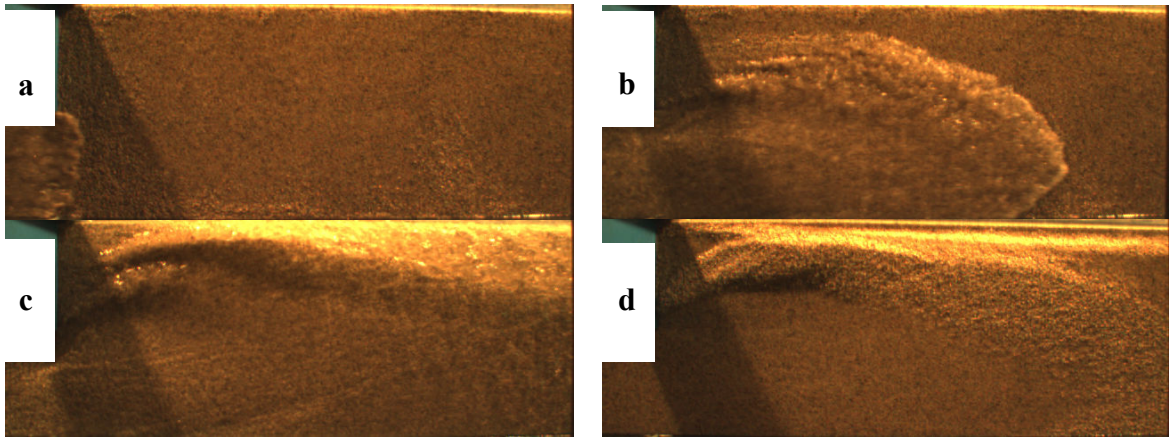

Fig. 5a-d. Top views of experiments with a sudden enlargement. a to c: times t = 0.5, 1.0 and 2.0 s. after gate opening, respectively. d: final bed topography emerging as the residual water is drained out.

Visible in Fig. 5a and b, the wave initially spreads in the wider region, and reflects against the opposite sidewall. The reflection evolves into an oblique hydraulic jump that slightly migrates upstream (Fig. 5c). Intense erosion occurs in the narrow section around the enlargement, and a scour hole develops at the inner corner of the widening. Part of the sediments are then deposited below the oblique jump, gradually forming a bar. As a side-effect, localised scour occurs very close to the sidewall due to the very turbulent boiling flow during the reflection. These features are illustrated by the final bed topography in Figure 5d.

4 MODEL SIMULATIONS AND COMPARISON

4.1 1D CONFIGURATION

We present simulation results obtained using the proposed 1D model, with the following parameter values: $_s$=2633 kg/m³; C_b=0.57; C_s=0.3; C_{fw}=0.02; C_{fs}=0.03; =30°; critical failure angle for the geostatic operator=30°; residual angle=14°.

Fig. 6 compares numerical profiles with the experimental observations. The profiles have been made dimensionless according to Froude similarity, and plotted at multiples of characteristic time $t_0 = (h_0/g)^{1/2}$ = 0.189 s. Good agreement is generally obtained. Initial failure and reshaping of the bed discontinuity is well reproduced (Fig. 6a), but the computed front celerity is slightly overestimated. This initial advance in the numerical wavefront vanishes as the wave progresses (Fig. 6b and c). The water levels and heights of the transport layer are correctly estimated. The weak hydraulic jump visible on the experimental profiles at later instants (Fig. 6d) is present in the simulations, but the latter is substantially sharper.

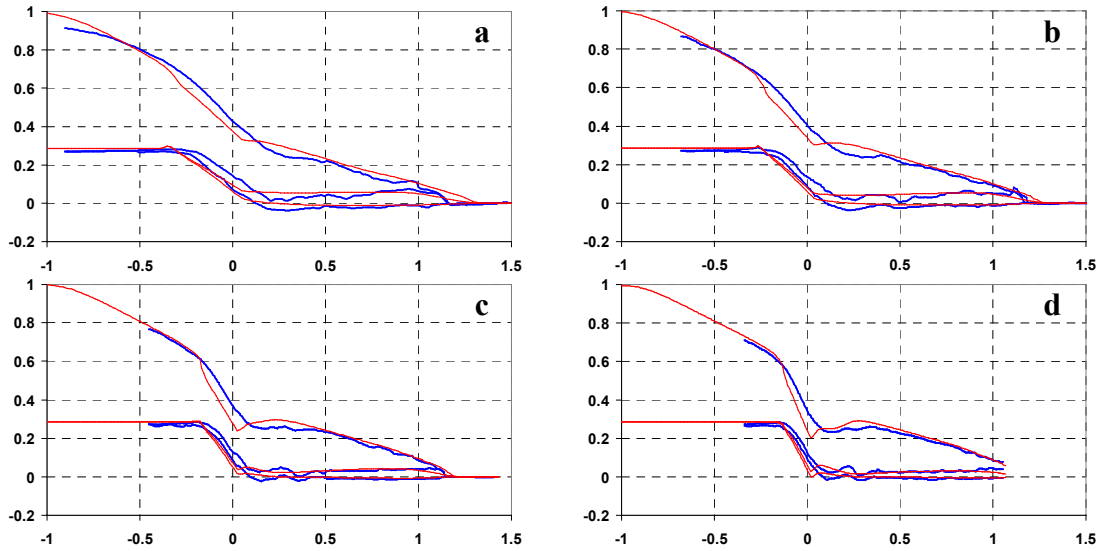

Fig. 6 a-d Experimental (blue) and modelled (red) flow profiles for the 1D configuration. Dimensionless ordinate z/h_0 , abscissa $x/(t(gh_0)^{0.5})$. a to d: profiles at times t = 3, 4, 6, and 8 t_0.

Fig. 7 compares sediment volumes transported throughout the flume and collected at the outlet. This provides a raw quantification for global geomorphic changes in the channel. The experimental value furnishes 2.63 kg, indicated as a straight line in Fig. 7. The numerical curve approaches the target value in a realistic way, though slightly overestimating it.

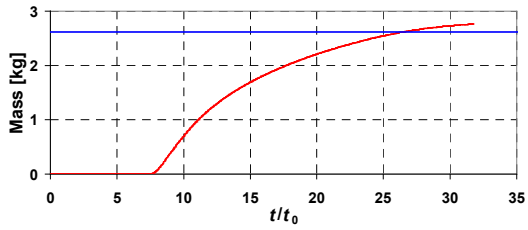

Fig. 7 Mass of sediments reaching the flume outlet as a function of time. The experimental blue line is the total mass gathered during the whole duration of the test.

4.2 2D CONFIGURATION

The triangular mesh used for the 2D simulation is shown in Fig. 8, and was generated using the Gmsh package (Geuzaine & Remacle, http://www.geuz.org/gmsh/). Cell size gradually evolves from 5 centimetres at the upstream end of the reservoir to 2 centimetres in the downstream reach. Additional local mesh refinement was provided in the neighbourhood of the inner corner at the sudden enlargement. Model parameters are as for the 1D simulation, except that, at the stage of those preliminary results, solid concentrations in the bed and transport layers were assumed equal, and that the geostatic failure operator was not activated.

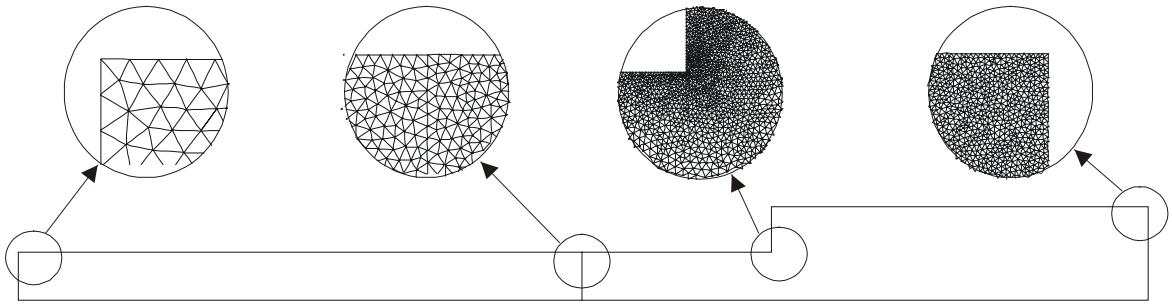

Fig. 8 The triangular computational mesh used in the computations.

Fig. 9 shows simulated flow snapshots at different instants. The simulation results on the triangular mesh have been interpolated on a coarser square grid for plotting purposes only. The successive reflections of the wave against the right (Fig. 9b) and left (Fig. 9c) sidewalls are clearly visible. Scour in the vicinity of the enlargement, as well as deposition below the oblique jumps, are in qualitative agreement with the experimental observations. Figure 10 provides a 3D impression of the simulated final bed topography, superimposed to a photograph taken after the test. Again, measurements of total sediment transport reaching the flume outlet were perform, with 2.05 kg for the experiment and 2.41 kg for the simulation.

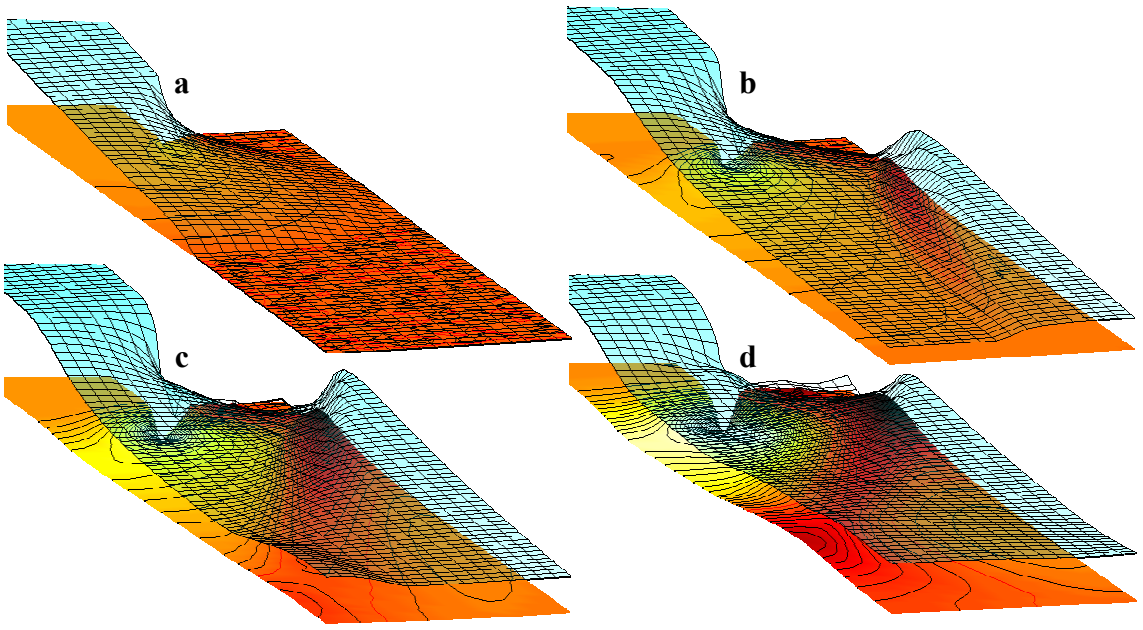

Fig. 9a-d Simulated flow snapshots at times t=1,2,3 and 5 seconds, respectively. The bed topography is shown through the translucent water surface, with depth contours every 1 mm.

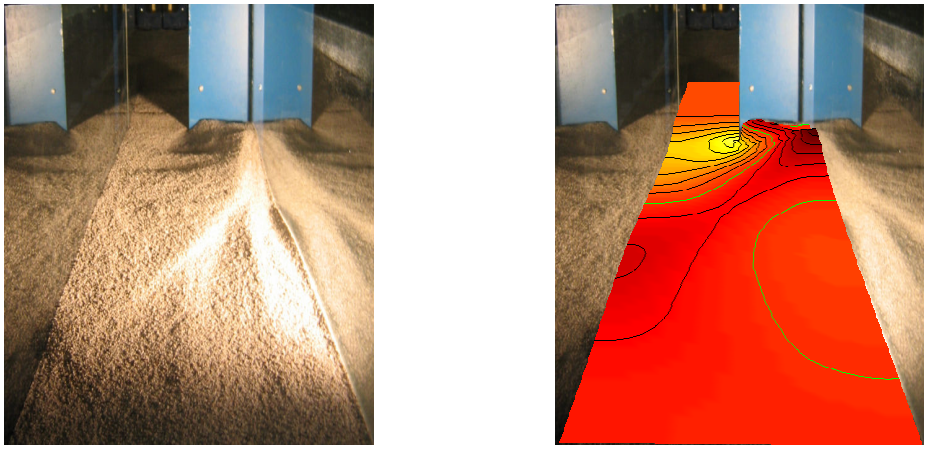

Fig. 10 Left: Downstream photograph of the final bed topography. Flow was from top to bottom. Right: simulated bed profile in superposition, with depth contours every 4 mm.

5. CONCLUSIONS

The paper presented a novel mathematical framework of governing equations for fast geomorphic flows, based on a two-layer shallow water description. An important innovation of the approach is to account for the reduction of granular concentration as a result of entrainment. The proposed model is validated based on two series of laboratory dam-break experiments, with generally good agreement. For the 1D configuration, an additional crucial element that explain this success is the incorporation of the geostatic slope failure operator that simulates the initial plastic failure of the bed discontinuity. For the 2D configuration, what we believe is a key factor of success is to allow sediment and water layers to flow in different directions, according to their momentum and interface topographies. This is particularly the case just downstream of the enlargement.

Current developments include trials to apply the approach to real-scale case-studies.

ACKNOWLEDGMENTS

The author wish to thank deeply his promoter, Pr. Y. Zech, and to express special thanks to H. Capart (National Taiwan University) and V. Guinot (Université Montpellier II), for their feed-back and encouragements, and for kindly making their numerical codes available.

REFERENCES

BROOKS G.R., LAWRENCE D.E. (1999) The drainage of Lake Ha!Ha! reservoir and downstream geomorphic impacts along Ha!Ha! River, Saguenay area, Quebec, Canada. Geomorphology 28: 141-168.

CAO Z., PENDER G., WALLIS S., CARLING P.A. (2004) Computatinal dam-break hydraulics over erodible sediment beds. J. Hydraulic Engineering, ASCE, 130(7):689

CAPART H. (2000) Dam-break induced geomorphic flows. PhD thesis, Université catholique de Louvain, Louvain-la-Neuve, Belgium.

CAPART H., YOUNG D.L. (2002) Two-layer shallow water computations of torrential geomorphic flows. Proceedings of River Flow 2002, Louvain-la-Neuve, Belgium, September 2002.

FERREIRA R., LEAL J., CARDOSO A.H., ALMEIDA A.B. (2003). Sediment Transport by Dam-Break Flows. A Conceptual Framework Drawn from the Theories for Rapid Granular Flows. In EC Contract EVG1-CT-2001-00037 IMPACT Investigation of Extreme Flood Processes and Uncertainty, Proceedings 3rd Project Workshop, Louvain-la-Neuve, Belgium 6-7 November 2003 (CD-ROM).

FRACCAROLLO L., CAPART H., ZECH Y. (2003) A Godunov method for the computation of erosional shallow water transient. Int. J. of Numerical Methods in Fluids, 41:951-976.

GALLINO G.L., PIERSON T.C. (1985). Pollalie Creek debris flow and subsequent dam-break flood of 1980, East Fork Hood River Basin, Oregon. U. S. Geological Survey Water Supply Paper 2273, 22 pages.

GUINOT (2003) Godunov-type schemes: An introduction for engineers. Elsevier

SPINEWINE B., CAPART H., LE GRELLE N., SOARES FRAZÃO S., ZECH Y. (2002) Experiments and computations of bankline retreat due to geomorphic dam-break floods. Proceedings of River Flow 2002, IAHR International Conference on Fluvial Hydraulics, Louvain-la-Neuve, Belgium, September 4-6, 2002. Balkema: pp. 651-661

SPINEWINE B., CAPART H., LARCHER M., ZECH Y. (2003) Three-dimensional Voronoï imaging methods for the measurement of near-wall particulate flows. Experiments in Fluids, 34(2): 227-241.

SPINEWINE B., ZECH Y. (2005) Dam-break on a movable bed in presence of an initial bed discontinuity. Laboratory experiments and simulations with a multi-layer shallow-water model. XXXI IAHR Congress, Seoul, September 11-16, 2005.